Oxidation catalysis on Pt and Au : complexity of simple chemistry

Spronsen, M.A. van

Chapter 5

Hydrophilic interaction between low-coordinated Au and water: H_2O/Au(310) studied with TPD and XPS

5.1 Introduction

Gold is one of few examples of transition metals with only minor industrial or technical applications. In fact, only ∼12 % of newly mined Au goes into industry, while the majority ends up as either jewelry or financial investment [145, 146]. The industrially used fraction is utilized because of its nobility and its resulting inertness to corrosion. However, modern research shows that this inertness is not guaranteed and significant chemical reactivity can be ascribed to Au [147–149].

The reactivity of metal surfaces is the central focus of heterogeneous catalysis. Its purpose is to facilitate the formation of many chemical products and to control the emission of pollutants. In this field, Au's remarkable reactivity was discovered by observing a high activity at low temperatures for CO oxidation [27]. In addition, interesting applications for Au as catalyst have been found in the water-gas shift reaction (WGSR) [150] and the selective oxidation of alcohols [151]. All examples show that Au must be dispersed into nanosized structures to show reactivity.

The enhanced reactivity of low-coordinated Au atoms is one of the explanations for the need of nanosized structures. These atoms can be found in steps and kinks, which are increasingly abundant in smaller nanoparticles. To test this hypothesis, we used a stepped Au single crystal for this work. This model catalyst has a high density of steps and, therefore, low-coordinated Au atoms. So, it can be considered a good model system for a nanoparticle catalyst in this respect. Because it is a single crystal, it does not suffer from complicating details (such as support effects and electronic effects due to nanoconfinement) and is perfectly suitable to probe just the effect of low coordination on the reactivity of Au.

A key aspect of gold catalysis is the role of H_2O. By adding H_2O vapor, it was found that the reactivity in CO oxidation can be enhanced [28]. The role of H_2O is even more important in the WGSR, in which it is one of the reactants. The intimate relation between H_2O and Au's reactivity stimulated research in understanding the details of this interaction on well-defined, single-crystal model catalysts both experimentally [152–163] and theoretically [159, 164–171] and on well-defined supported Au clusters (for example see Reference 172).

This effort fits into a wider framework to understand the interaction between H_2O and solid surfaces. This interaction has become the subject of one of the most widely studied fields in surface science. Motivations for these studies are almost as numerous as the number of studies themselves. For example, it is also crucial to environmental chemistry, interstellar nucleation of ice particles, material corrosion, and electrochemistry in which H_2O is the most used solvent.

The interaction of H_2O with transition metals has been reviewed multiple times [173–176]. The early results were believed to widely support an extended-bilayer model. This frequently proposed bilayer model was not able to explain all results obtained with newly developed tools, most notably scanning tunneling microscopy (STM), combined with density functional theory (DFT). These studies led to interesting cases in which the bilayer model was simply incorrect and the structures formed were more complex and beautiful. An important case is the extended overlayer formed on Pt(111). This layer contained pentagonal, hexagonal, and heptagonal rings [177–179].

Even more interesting, one-dimensional (1D) structures can form when the considered surface is anisotropic. This is well illustrated on Cu(110) on which intact H_2O forms chains from pentagons in the $[00\bar{1}]$ direction [180, 181]. Furthermore, partially dissociated H_2O forms chains in the $[\bar{1}10]$ direction [182]. This anisotropy can be strengthened by going from flat to vicinal surfaces.

The interaction between H_2O and stepped surfaces was the focus of a number of studies. Steps generally show a stronger interaction with H_2O as determined with temperature-programmed desorption (TPD) on Pt [183–186], Ru [187, 188], Ni [189], and Co [190]. The experimental work was supported by computational studies on Pt [184, 191–194], Cu [195, 196], and Ni [197, 198]. Although the precise orientation of the steps play an important role, details have not been fully understood yet [184–186, 194, 199–201]. In addition to binding H_2O more strongly, steps also lower the dissociation barrier on Pt [191–194], Cu [196], Ni [189, 198, 202], Ru [188], Co [190], and Re [203]. Interestingly, the steps of Pt were observed to be covered by 1D chains [199, 204, 205].

The focus of the present work is to study how anisotropy influences the binding of H_2O with the much nobler Au and to see if a weakly interacting surface can also show enhanced binding and 1D structures. Of especial interest is the question whether steps are able to dissociate H_2O to any observable extent. To study these effects, care was taken to choose one of the most open and expectedly reactive surfaces. This led to the Au(310) surface, which can be considered as a highly stepped (100) surface with steps forming (110) planes. The adsorption and desorption was studied both with TPD and high-resolution X-ray photoelectron spectroscopy (XPS).

5.2 Experimental

The (310) surface is depicted in Figure 5.1a–c, showing the single (110) steps and 2 or 3 atom wide (100) terraces. The atoms in this surface have a coordination number which varies between 6 for the atoms in the ridge of the (110) step to 8 in the (100) terrace and 9 at the base of the (110) step. Both the coordination numbers and the surface unit cell are given in Figure 5.1.

Two different Au single crystals were used and polished to the (310) surface with an accuracy of $< 0.1^\circ$ [41] (for the TPD measurements) and $\sim 2.3^\circ$ (for the XPS measurements). To obtain a well-defined and clean surface, the crystals were prepared by Ar^+ sputtering with an energy of 500 eV for the TPD experiments and 1 keV for the XPS experiments for a few minutes. Sputtering was followed by annealing in vacuum at 860 K. Multiple cycles resulted in a contaminant-free and well-ordered surface confirmed by low-energy electron diffraction (LEED) and XPS. After preparing the crystal, the surface structure was checked with LEED. A photograph of a typical diffraction pattern is shown in Figure 5.1d. It was recorded with a beam energy of 60 eV and colors were inverted for clarity. In the LEED pattern, the spot splitting arising from the stepped surface was clearly observed. The ratio of spot row spacing to split spot distance was 1.54 ± 0.2. This was close to the theoretical value of 1.58 [207]. The LEED patterns did not show any sign of a surface reconstruction. This was in

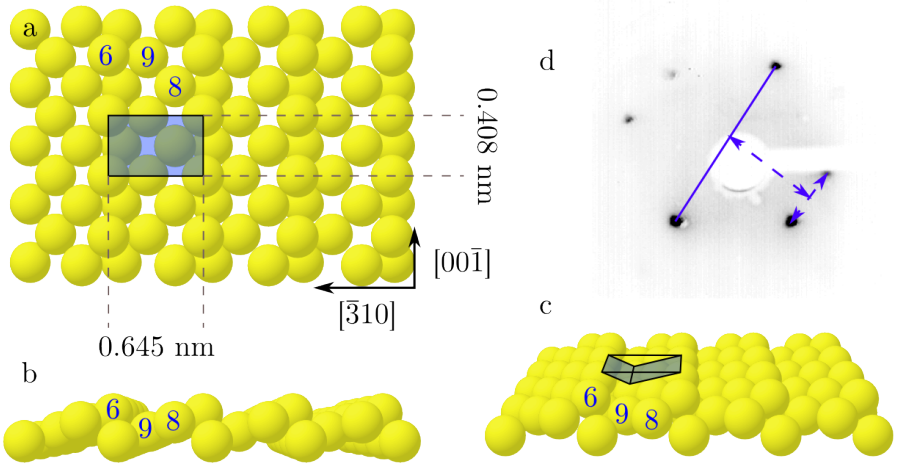

Figure 5.1: Three views, (a)–(c), of a ball model [206] of the (310) surface of a face-centered cubic crystal, such as Au. The indicated surface unit cell measures 0.408×0.645 nm^2. Atoms with different coordination numbers are depicted. (d) shows a color-inverted LEED photograph of clean Au(310) at 60 eV electron energy. In the LEED image, the distances are indicated to measure the ratio between spot splitting and row spacing.

good agreement with the STM results of Weststrate et al. [208].

High-purity[1] H_2O was used for the TPD experiments. It was degassed by multiple freeze-pump-thaw cycles until a quadrupole mass spectrometer (QMS) confirmed the absence of O_2. Small amounts of N_2 were considered to be irrelevant, due to the expected inertness of Au to N_2. The degassed H_2O was admitted via a capillary array doser [209]. It was co-dosed with high-purity[2] He at ∼1.5 bar at room temperature. This resulted in a mixture containing ∼1.5 % H_2O. Co-dosing of He was used to create reliable and repeatable pressure readings. For the XPS experiments, high-purity[3] D_2O was used, which was prepared and dosed in the same way. The dose was reported in Langmuir (L), defined as 1×10^{-6} Torr s. The pressure was measured with a hot-filament ionization gauge. No gas-specific corrections were applied, because for H_2O these correction factors are close to and scattered around 1 [210].

Experimental work was performed using two different ultra-high vacuum (UHV) systems, one was used for the TPD experiments[4] and the other for the XPS experiments[5]. The TPD setup was equipped with a LEED[6] system and a QMS[7], mounted directly on the main chamber. The main chamber was evacuated with two turbomolecular

[1] Milli-Q Ultrapure
[2] 6.6 N purity
[3] 99.96 at.% D, Aldrich
[4] Chemistry department, Leiden University, the Netherlands
[5] SuperESCA beamline, Elettra, Trieste, Italy
[6] VG RVL 900
[7] Baltzers Prisma 200

pumps in series. These pumps ensured a base pressure of $(1–2)\times10^{-10}$ mbar.

The sample was mounted on a multistage manipulator containing a liquid-nitrogen cryostat, cooling the sample down to 88 K. The sample was heated by a filament mounted close to the rear of the crystal, combining thermal radiation with electron-beam heating. The temperature was measured by a chromel/alumel thermocouple laser spot welded to the side of the crystal. The temperature was controlled with a PID controller[8] to create linear temperature ramps needed for the TPD experiments.

All TPD traces reported in this work were obtained with a heating rate of ∼0.9 K/s. Adsorption of H_2O and subsequent desorption from the walls of the chamber resulted in enhanced background levels during a measurement. This unavoidable behavior was corrected using a hyperbolic tangent to describe the change in background level [186].

The XPS measurements were performed at the SuperESCA beamline, Elettra synchrotron, Trieste, Italy [211]. This beamline is designed to give a high-intensity, monochromated X-ray beam tunable between roughly 0.1 and 2 keV.

XP spectra were collected at normal emission and at a beam angle of 70°. The Au $4f_{7/2}$ signals were recorded with a photon energy of 170 eV and a dwell time of 50 ms and 650 eV with 30 ms for the O 1s signal. Both the Au $4f_{7/2}$ and O 1s signals were measured in a constant-energy analyzer mode with a pass energy of 4.0 and 15.0 eV, respectively. Moreover, the hemispherical analyzer was set to medium-area mode.

The obtained XP spectra were compensated for changes in beam flux and differences in dwell time by dividing the spectra by a linear background. The XP peaks were fitted with a Doniach-Šunjić function [94] convoluted with a Gaussian line shape. This fitting function required the following fitting parameters: binding energy, intensity, Lorentzian line width, Gaussian line width, and asymmetry factor. Fitting parameters were accepted if a time-resolved data set could be successfully fitted with only the intensities as free fitting parameters. The XP binding energies are reported with respect to the Fermi level. This was measured every time after switching to a different photon energy. The uncertainty in the fitted binding energies is estimated to be around 50 meV.

The O 1s signal was quantified in two separate ways. First, it was calibrated by the O 1s signal from a CO-saturated surface at 105 K. CO adsorption saturates when half of the step sites are covered, which occurs at 0.167 ML [161, 208]. This calibration was performed both for a photon energy of 650 and 1205 eV, which agreed within 11–12 %. Second, the surface concentration ratio between the D_2O layer and the Au surface was calculated with [212]

$$\frac{N_{D_2O,surf}}{N_{Au,surf}} = \frac{\sigma_{Au4f}\lambda_{Au}[1-\exp(-\frac{d_{Au}}{\lambda_{Au}})]}{\sigma_{O1s}\lambda_{D_2O}[1-\exp(-\frac{d_{D_2O}}{\lambda_{D_2O}})]}\frac{I_{O1s}}{I_{Au4f,\ surf}}$$

in which σ are the respective ionization cross sections, which were linearly interpolated for the correct photon energy from the values reported by Yeh and Lindau [213]. The recommended, practical effective attenuation length, λ, for Au (0.34 nm) was taken from the NIST database [214] and the reported values for solid

[8] Eurotherm 2416

water (1.8 nm [215]) were used. In this formula, d is the layer thickness, 0.193 nm for a Au layer. The water layer thickness on Au has been measured with STM and values of 0.11–0.15 nm [156, 159] have been found, although 0.25 nm was found with helium atom scattering [163]. Values between 0.11–0.15 nm were used for our calculations. In this calculation, the asymmetry factor was assumed to be 1 and the transmission function of the analyzer constant, due to the small (∼32 eV) difference in kinetic energy of the emitted photoelectrons. Both methods gave similar values within ∼20 %.

Small amounts of amorphous C were detected during the XPS experiments. This was attributed to beam damage, more specifically to cracking of C-containing gas molecules. However, typical amounts were just at the XPS detection level and they were monitored frequently during the experiment. If the C contamination was significantly increasing, the experiment was aborted and the cleaning procedure repeated.

5.3 Results

5.3.1 TPD experiments

Figure 5.2 shows the results of the TPD experiments obtained after adsorbing various amounts of H_2O on Au(310) at a surface temperature of ∼90 K. For low coverages, a single feature was observed (blue traces, Figure 5.2), labeled as peak α. For this peak, the leading edges for different doses completely overlap. Furthermore, the temperature at maximum desorption, i.e., the desorption temperature, increases from about 158 to 170 K. Both properties indicated complicated desorption kinetics and a desorption order of less than 1.

When the H_2O dose was increased above 1.0 L, a second peak (peak β) emerged at the low-temperature side. This new peak appeared, while peak α was not fully saturated. The characteristics of this second peak were very similar to those of peak α, i.e., overlapping leading edges and increasing desorption temperature (from 161 to 168 K). It is noteworthy that there was no saturation observed up to the maximum H_2O dose. The inset of Figure 5.2 shows one example of the hyperbolic tangent used to fit the increasing background pressure during the experiment [186].

A TPD simulation was performed to gain further insight into the observed desorption kinetics. This simulation is included as supplementary information (see Figure 5.14). The comparison between experiment and simulation revealed that desorption followed zero-order kinetics. All together, these results were in very good agreement with van Reijzen et al. [161].

The results are in qualitative agreement with desorption from Au(110) [153]. However, the measured desorption temperatures from that surface were much higher, 185 and 190 K. This difference cannot be completely explained by the higher heating rate used in that work (3 K/s versus 0.9 K/s in this work). A shift to higher desorption temperatures could also be due to stabilization by (partially) dissociated H_2O or contamination. Also, there is little structural resemblance with Au(310) due to the missing-row reconstruction present on Au(110). Therefore, we will not further discuss the comparison between Au(310) and Au(110).

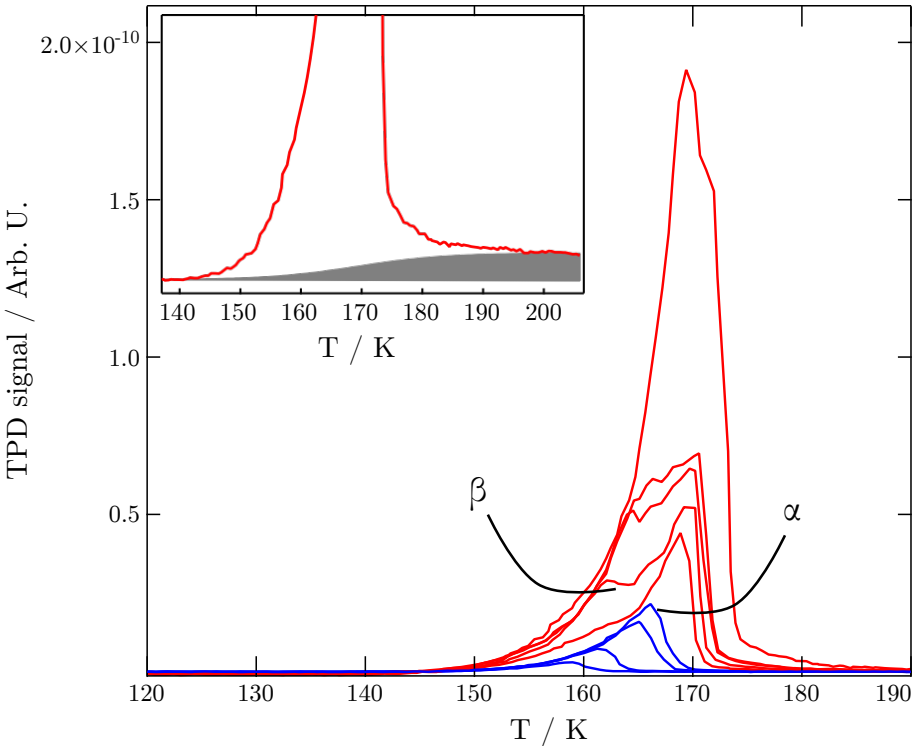

Figure 5.2: TPD traces of various doses of H_2O adsorbed at ~90 K, recorded with a heating rate of ~0.9 K/s. Blue traces showed only peak α. Red traces showed, in addition, desorption of H_2O from a second, lower-temperature peak, β. The inset shows an example of a background correction, fitted with a hyperbolic tangent. This accounted for the increase in pressure after the desorption and originated from the low pumping speed of H_2O.

Peak fitting

To separate the peaks and calculate adsorption energies for both TPD peaks, a polynomial function was fitted through the overlapping leading edges of peak α. This polynomial was extended and subtracted from traces showing both features, resulting in two separate peaks. These are plotted in Figure 5.3a, peak α, and Figure 5.3b, peak β.

The separation appeared to produce a reasonable result at first glance. For higher coverages, however, the right-hand side of peak β in Figure 5.3b intersected the x axis almost perpendicularly. Although this behavior is predicted for zero-order desorption, it appeared to be too perfect. Also, peak α did not seem to saturate up to 3 L, which could be an artifact of the separation procedure.

The insets of these panels show the change in desorption temperature as a function of the integrated TPD signal. Furthermore, the integrated TPD signals of the total signal (red), peak α (blue), and peak β (green) plotted versus the H_2O dose are

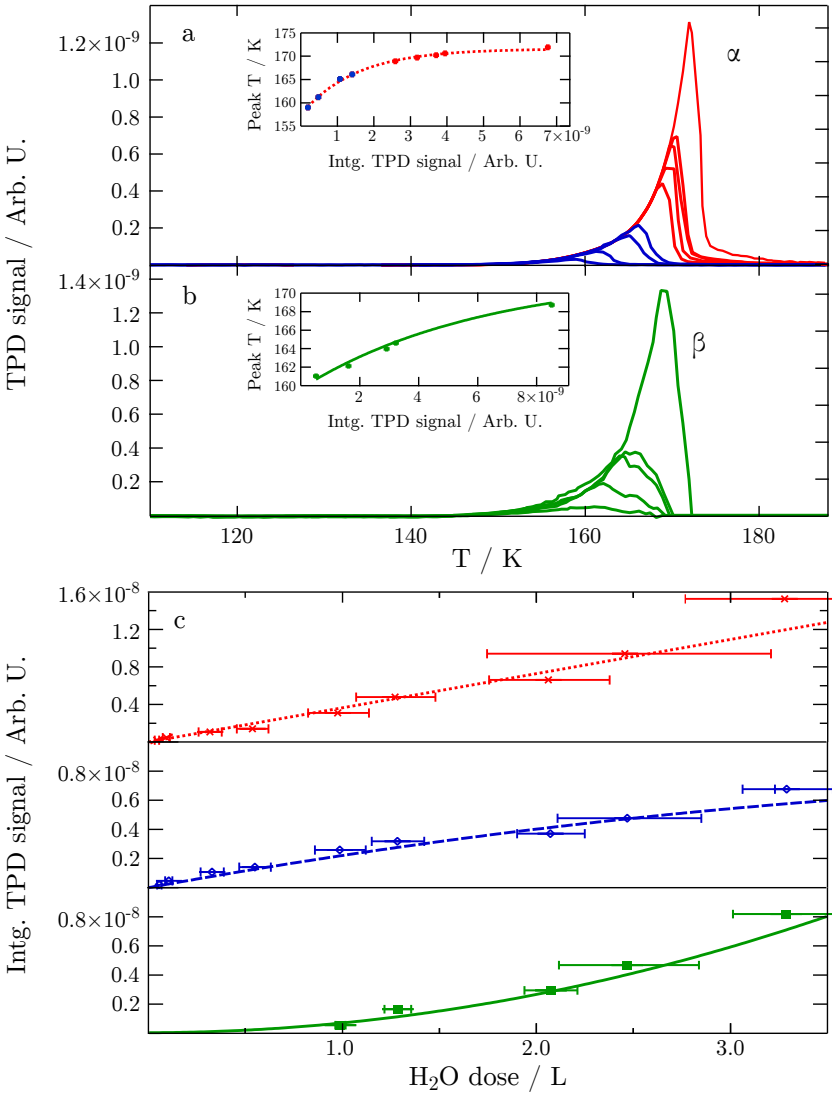

Figure 5.3: Separation of the two desorption features: (a), peak α, ascribed to H_2O directly bonded with Au and (b) peak β, low-temperature peak associated with H_2O multilayers. The separation was performed by fitting a polynomial through the leading edges of traces with a single desorption feature (blue traces, (a)) and subtracting the integrated fit from desorption traces showing both features. The insets of (a) and (b) show the peak temperature versus the integrated TPD signal. (c) shows the integrated TPD signals plotted versus H_2O dose for the total TPD signal (red trace), peak α (blue trace), and peak β (green trace).

shown in Figure 5.3c. In this graph, the estimated error on the dose was based on moderate pressure variations and time inaccuracy and scale with increasing dose. The data for both peaks α and β were fitted with a polynomial function to guide the eye.

From this graph, the coverage dependence of the sticking coefficient could be derived. The sticking coefficient of peak α was decreasing with increasing dose, while the sticking coefficient of peak β was increasing.

Leading-edge analysis

A leading-edge analysis was performed to obtain the adsorption energy of the two TPD peaks. This analysis is shown in Figure 5.4. The leading-edge analysis consisted of plotting the natural logarithm of the TPD signal versus the inverse temperature. Its slope gave the adsorption energy under the assumption of zero-order desorption according to the Polanyi-Wigner equation:

$$\ln(\text{TPD signal}) = (-E_a/R)T^{-1} + C$$

In this equation, E_a is the adsorption energy, R is the gas constant, T is the temperature, and C is a constant depending on the pre-exponential factor and some experimental constants, such as the sensitivity of the QMS and the pumping speed of the system. In this graph, the original TPD data are also shown on a linear scale (right axis) and the upper axis reads the temperature.

Because the leading edges were overlapping for both peaks, a single TPD trace per peak was analyzed. Specifically, the adsorption energy for peak α was calculated with the highest TPD trace that was showing a single peak. For peak β on the other hand, the maximum TPD trace was used to minimize the relative contribution of peak α. This resulted in adsorption energies of 55 ± 2 kJ/mol for peak α and 48 ± 1 kJ/mol for peak β.

5.3.2 XPS experiments

O 1s during adsorption

Figure 5.5 shows the O 1s XPS signal with increasing amounts of adsorbed D_2O. A single and asymmetric peak was visible at very low D_2O dose. With increasing D_2O exposure, the asymmetry decreased and the peak shifted to higher binding energy.

The dose-dependent O 1s signal was further investigated by plotting the integrated O 1s signal (top panel, Figure 5.6) and the peak binding energy (lower panel, Figure 5.6) versus the D_2O dose. The integrated O 1s signal was linearly increasing with the D_2O dose in accordance with the TPD data (Figure 5.3c). However, the slope decreased by a factor of 1.7 above 0.5 L at a coverage of 1.1 ML. It can be partially explained by the onset of the growth of the second layer of D_2O. This layer shielded photoelectrons emitted by the first layer resulting in a lower total growth rate. However, this only accounts for a decrease with a factor of roughly $1/(\exp(-\frac{d_{D_2O}}{\lambda}) = 1.06$–$1.09$. So, it is likely that the sticking coefficient of the second layer decreased with a factor of 1.6.

Additionally, the binding energy showed an abrupt change. This change occurred at somewhat lower dose (0.4 L) at a coverage of 0.8 ML. At lower dose, the binding

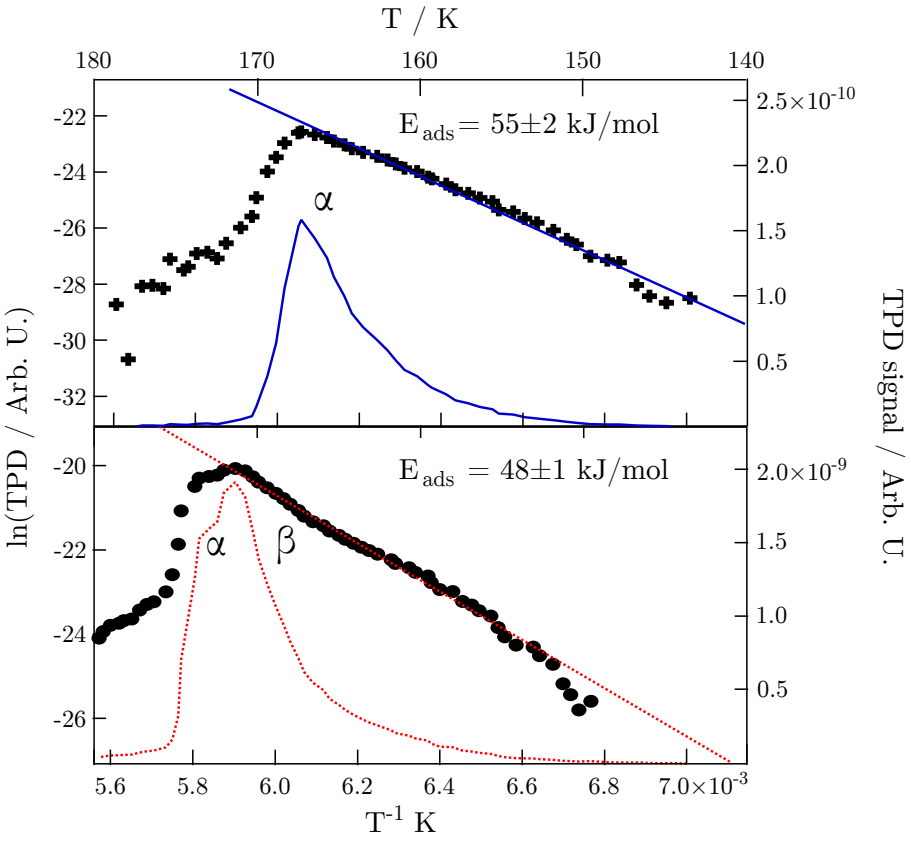

Figure 5.4: Polanyi-Wigner analysis to obtain the adsorption energy. Ln(TPD signal) was plotted versus T^{-1}. The slope of the leading edges gives the adsorption energy. This resulted in 55 ± 2 and 48 ± 1 kJ/mol for peak α (blue, solid) and β (red, dotted), respectively. For clarity, the original TPD signal was also plotted against temperature (top axis).

energy was constant at 532.3 eV; at higher dose, it gradually shifted to 532.8 eV. We attribute this change also to the growth of the second layer of D_2O.

A more detailed understanding was derived from the model used to fit the O 1s XPS data. The results are presented in Figures 5.7 and 5.8. In this model, the D_2O adsorption is essentially explained by the population of two different O 1s states, one is D_2O directly bonded to the Au surface (532.2 eV) and the other is a multilayer D_2O state (532.8 eV). The results of these fits are illustrated in Figure 5.7a and 5.7b for 0.1 and 1.6 L D_2O. These figures demonstrate that satisfactory fits were obtained as indicated by the small fitting error, depicted in the lower part of the graphs. In addition, a small peak was fitted at 529.9 eV. This minority species accounted for roughly 1% of the total O 1s signal and was assigned to atomic oxygen. This feature could stem from dissociation of D_2O as a result of beam damage or by defects in

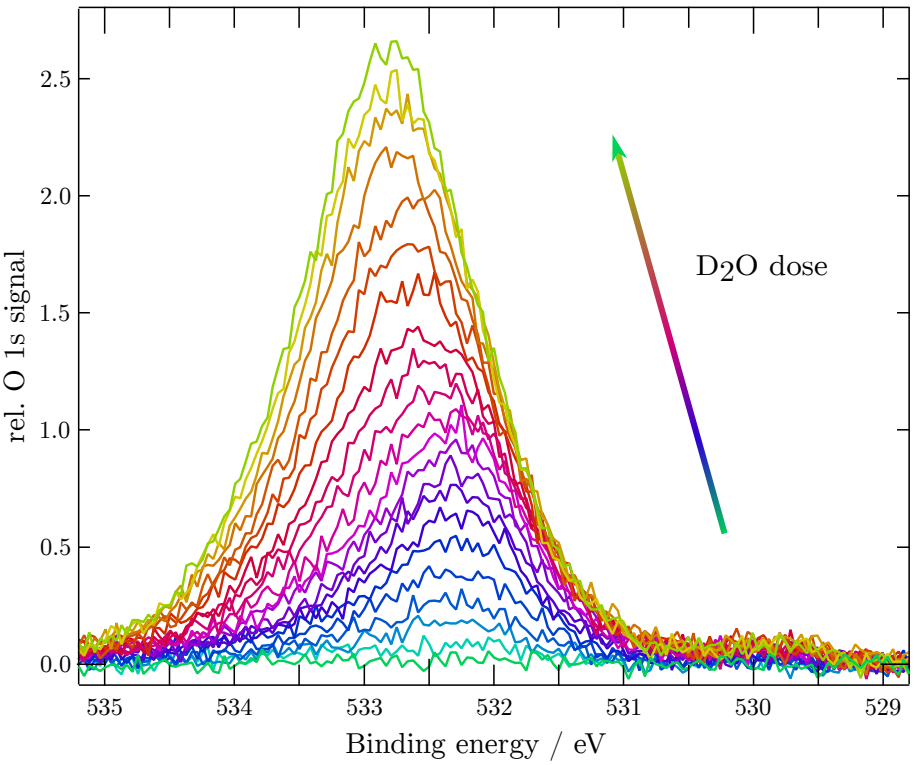

Figure 5.5: O 1s signal from a clean surface up to high D_2O coverage (blue to green traces) during the D_2O adsorption, ranging from 0 to 1.7 L D_2O at 106–103 K.

the Au(310) surface with an even lower coordination number.

The resulting peak areas are plotted against the D_2O dose in Figure 5.8 and show that the multilayer D_2O started to appear from the smallest D_2O dose onward. Furthermore, Figure 5.8 shows that a change of growth rate occurred at a dose of 0.4 L, above which growth of multilayers increased. However, the precise coverage where this switch occurred was rather dependent on the values taken for the fitting parameters. In any case, the trend of populating the peak at 532.8 eV even for the lowest D_2O dose was robust with respect to differences in fitting parameters. This is an interesting feature, which will be explored further in the discussion.

Au $4f_{7/2}$ during adsorption

With the focus switched to the Au $4f_{7/2}$ signal, the D_2O adsorption experiments were repeated. The Au $4f_{7/2}$ spectra with increasing D_2O coverages are shown in Figure 5.9, revealing that the Au $4f_{7/2}$ signal was gradually decreasing upon D_2O adsorption. This

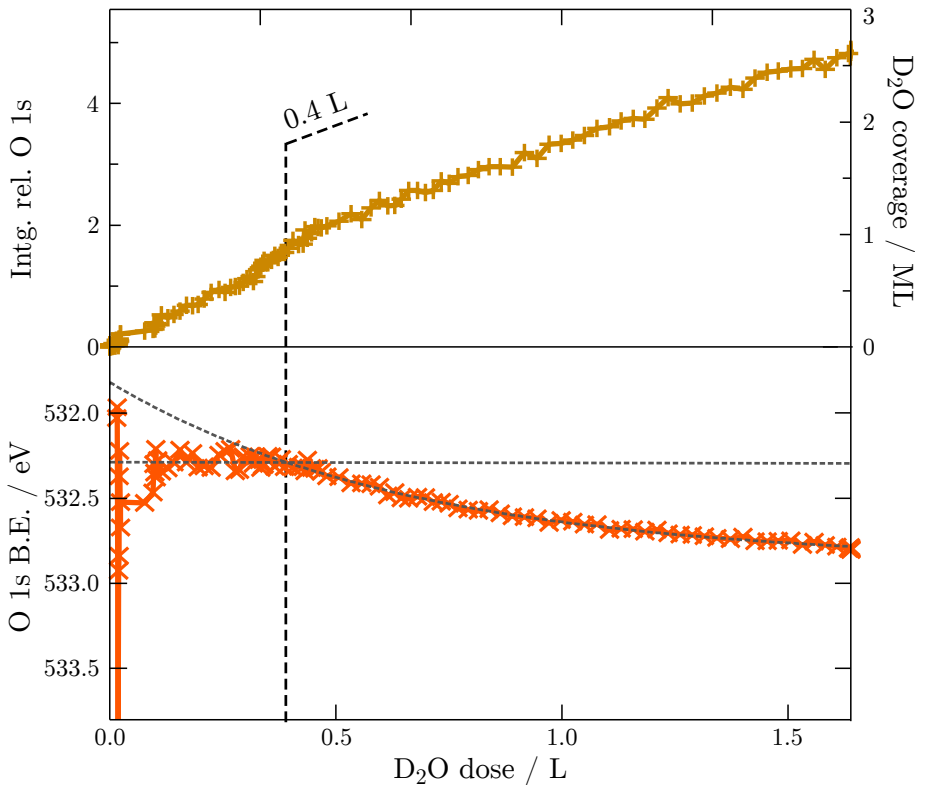

Figure 5.6: Integrated XPS signal (brown, pluses) and the binding energy (orange, crosses) plotted versus D_2O dose. The coverage increased linearly, however, with a lower rate above ~0.5 L. As the coverage increased (above 0.4 L), the binding energy started shifting to higher values (from 532.3 to 532.8 eV).

tendency can be attributed to shielding of the Au atoms by D_2O. However, the shape of the Au $4f_{7/2}$ features significantly changed with increasing dose. This was most clearly visible by the loss of separation between the peak at 84.0 eV and the shoulder at 83.4 eV. The integrated Au $4f_{7/2}$ signal showed clear correlation with the D_2O dose as displayed in Figure 5.10. The integrated signal was linearly decreasing, when D_2O was admitted in the vacuum chamber (indicated by vertical, dashed line in Figure 5.10).

A model to fit the Au $4f_{7/2}$ data was harder to establish. In principle, one could expect contributions from atoms with the three different coordination numbers. However, both the relative intensity and the core-level shift are not known for this particular stepped surface and material. In fact, research did show that there is not always a direct relation between coordination number and the magnitude of the core-level shift [216, 217]. Furthermore, the relative intensities depend at least on photon energy, detector angle, and step alignment with respect to the plane defined by the

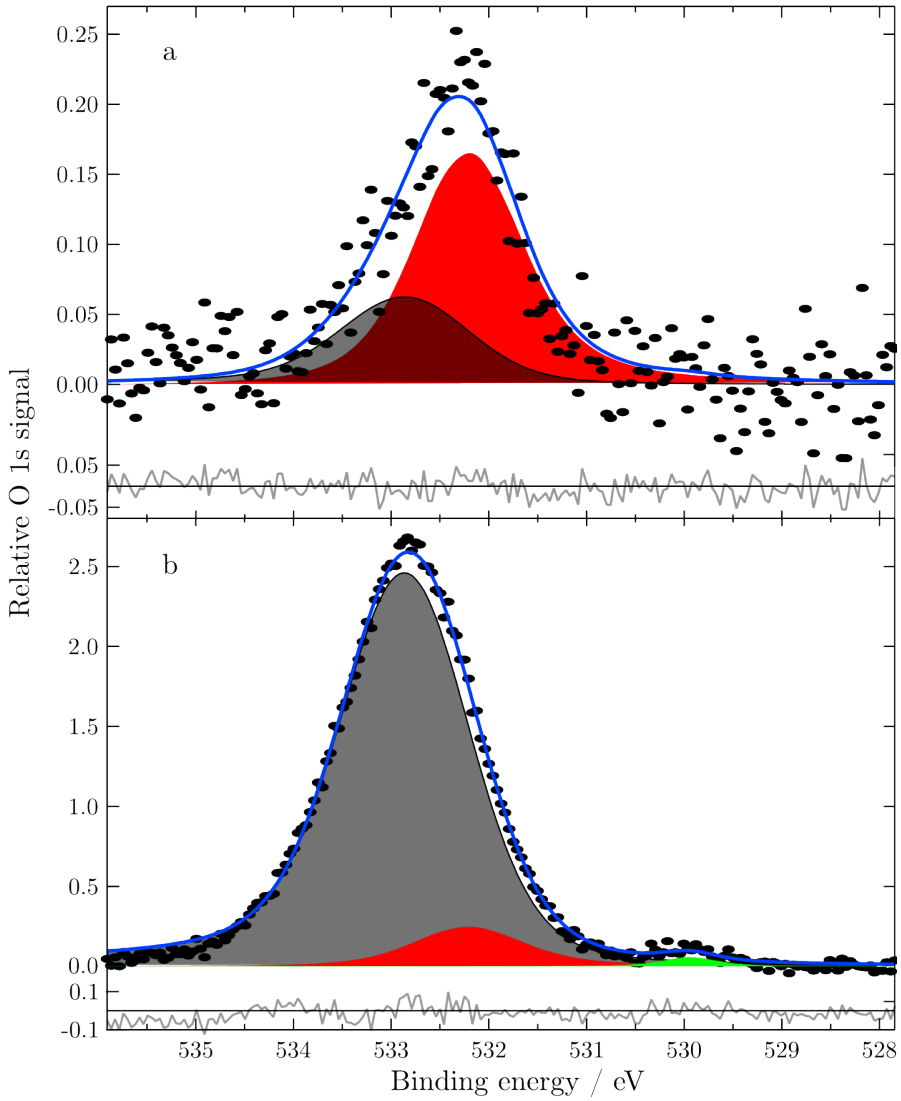

Figure 5.7: Two fitting examples, (a), low D_2O dose (0.1 L), and (b) higher D_2O coverage (1.6 L). The fitted peaks represented monolayer D_2O (red, 532.2 eV), 'multilayer' D_2O (black, 532.8 eV) and atomic O peak (green, 529.9 eV). In the lower part, the difference between data and fit is shown.

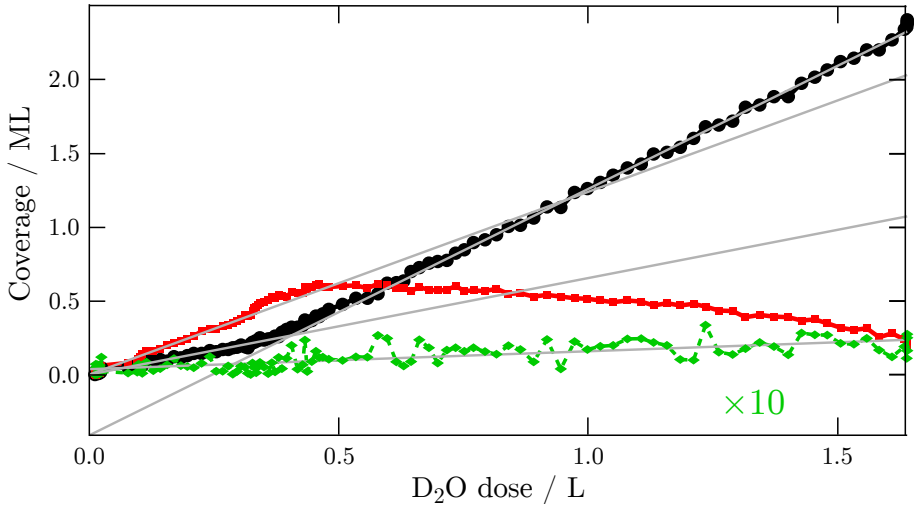

Figure 5.8: Coverages of different oxygen-containing species on the surface during adsorption of 1.6 L D_2O. Fit model consisted of monolayer D_2O (red, solid squares, 532.2 eV), 'multilayer' D_2O (black, solid circles, 532.8 eV) and a minute atomic O peak (green, dashed, solid diamonds, 529.9 eV). From low doses on, 'multilayer' D_2O was growing and around 0.9 ML a step increase in the growth rate was visible. Around 0.5 L, the intensity of the monolayer started decreasing due to screening by the second layer.

X-ray beam and detector [218, 219]. The intensities could also depend on the incident angle of the X-ray beam. In conclusion, there are too many unknown parameters to yield a detailed fitting model without further research into Au surface core-level shifts.

To circumvent these difficulties, a simplified model was used consisting of only one peak for all surface contributions. The results are depicted in Figure 5.11 and it shows that a fairly reasonable fit was obtained. The core-level shift of the surface atoms with respect to bulk Au was found to be 0.42 eV. This shift was larger than shifts reported for the closed-packed Au surfaces (0.28–0.38) [216] and, in line with our expectation, resembles the shift obtained from polycrystalline Au (0.39 ± 0.05) [220].

Upon D_2O adsorption, one expects a new Au species to appear originating from surface Au atoms interacting with D_2O. As we represent the surface Au atoms by a single peak, we add one additional, independent Doniach-Šunjić functional form to represent the changes upon D_2O adsorption. The chemical shift between the clean Au atoms and the ones interacting with D_2O is only 0.1 eV as shown in (Figure 5.11b). This suggests a very weak interaction between Au and D_2O.

Figure 5.12 shows the fitted peak areas versus dose. It shows that the contribution from surface Au atoms gradually decreased and stayed constant above 0.8 L at approximately half of the original value. Simultaneous to this decrease, the peak attributed to D_2O-Au increased, while remaining constant above 0.8 L.

We propose that the first D_2O layer accumulated to around 0.8 L. Half the surface Au atoms interacted with the molecules in this layer. The second layer had little

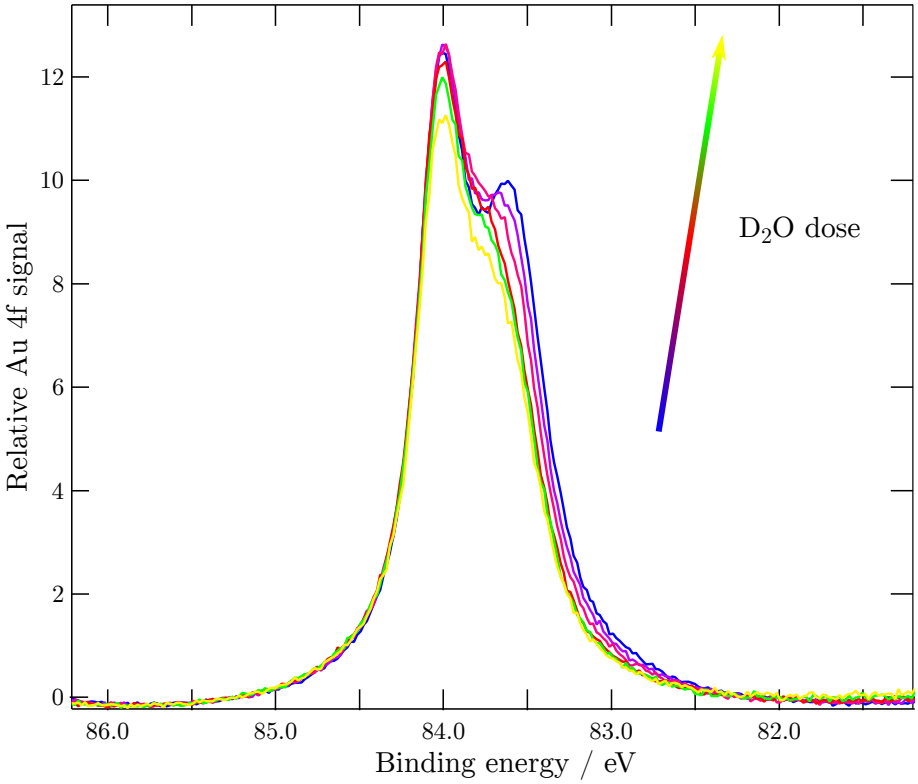

Figure 5.9: Au $4f_{7/2}$ signal from clean (blue) to high D_2O coverage (yellow) during adsorption of a D_2O dose ranging from 0 to 1.5 L at 108–104 K. The clean surface showed a peak at 84.0 eV assigned to bulk Au and an intense shoulder at 83.4 eV due to surface Au atoms.

interaction with the Au surface. Therefore, the second layer induced no further shape change to the Au $4f_{7/2}$ spectra and only accounted for further shielding of the photoelectrons emitted by the Au atoms.

O 1s and Au $4f_{7/2}$ during desorption

In the final set of the experiments, the XPS signals were monitored during D_2O desorption. In these experiments, the surface temperature was linearly increased with 0.10 K/s. The results are presented in Figure 5.13. The areas of the two fitted O 1s peaks are shown as a function of temperature in Figure 5.13a, while Figure 5.13b shows the areas of the three fitted Au $4f_{7/2}$ peaks. During the temperature ramp, multilayer D_2O started to desorb around 142–144 K. Desorption of this feature was observed by a decrease in the corresponding O 1s signal (Figure 5.13a) and an increase in all the Au $4f_{7/2}$ peaks (Figure 5.13b). This was attributed to decreased shielding

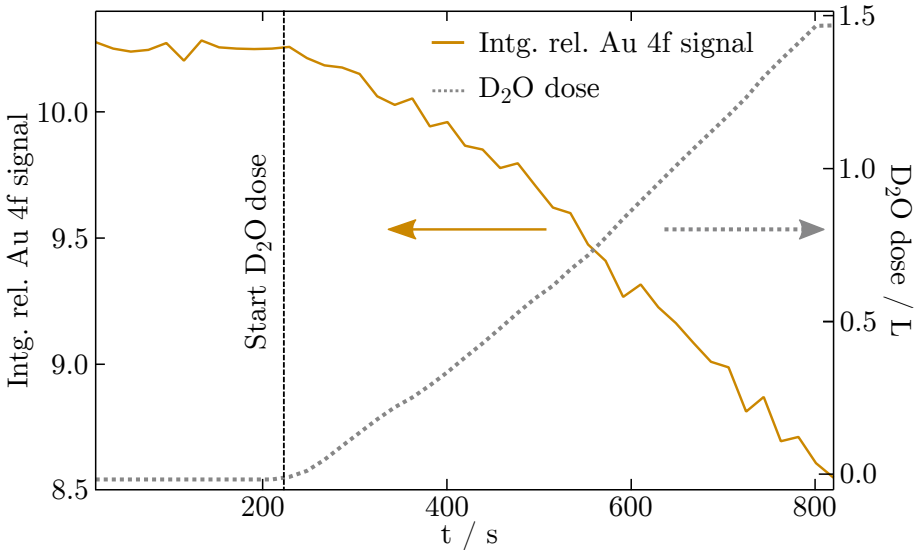

Figure 5.10: Integrated Au $4f_{7/2}$ signal (brown, solid) and D_2O dose (gray, dotted) plotted versus time. The total integrated signal decreased with increasing D_2O dose.

of the diminishing D_2O layer. Multilayer desorption was followed by desorption of monolayer D_2O at slightly higher temperature, starting at 153–155 K.

Temperature derivatives of these signals are plotted below the respective graphs. These derivatives correspond to the desorption rates and are plotted in such a way that these rates are all positive. These desorption rates showed good resemblance with the TPD experiments (Figures 5.2 and 5.3), although desorption temperatures were about 10 K lower. This difference can be explained by the lower heating rate (0.1 K/s instead of 0.9 K/s) resulting in a 10 K shift as confirmed by the numerical TPD calculations.

5.4 Discussion

5.4.1 Intact or dissociative adsorption

The dissociation of H_2O was found to be exothermic on Au(111) and proceeding at high temperature (>750 K) [152]. Furthermore, steps are known to bind H_2O more strongly and lower the dissociation barrier [183–205]. However, is this effect strong enough to allow for sufficient H_2O dissociation below the desorption temperature on Au(310)? The TPD measurements (Figure 5.2) give the first indication that this is not the case. The high-temperature peak α showed zero-order desorption, which would not be expected from desorption of fragmented H_2O. On Au(111) and Au(110), an additional peak was observed after coadsorption of water and O_{ad} [153, 221, 222]. This peak was 20–30 K higher in desorption temperature compared to the desorption

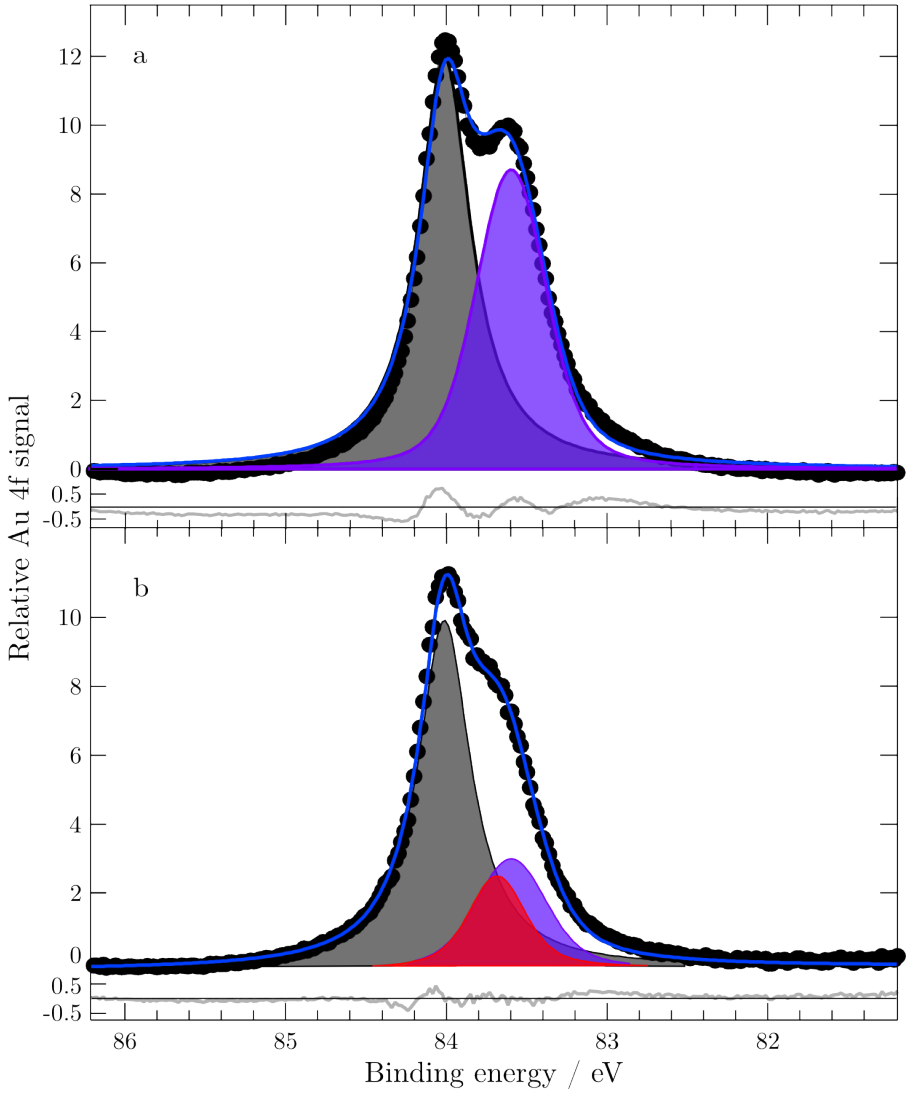

Figure 5.11: Two fitting examples: clean Au (a), and high D_2O coverage, 1.5 L (b). Peaks represent bulk Au (black, 84.0 eV), surface Au (blue, 83.6 eV), and D_2O-bonded Au (red, 83.7 eV). In the lower part, the difference between data and fit is shown.

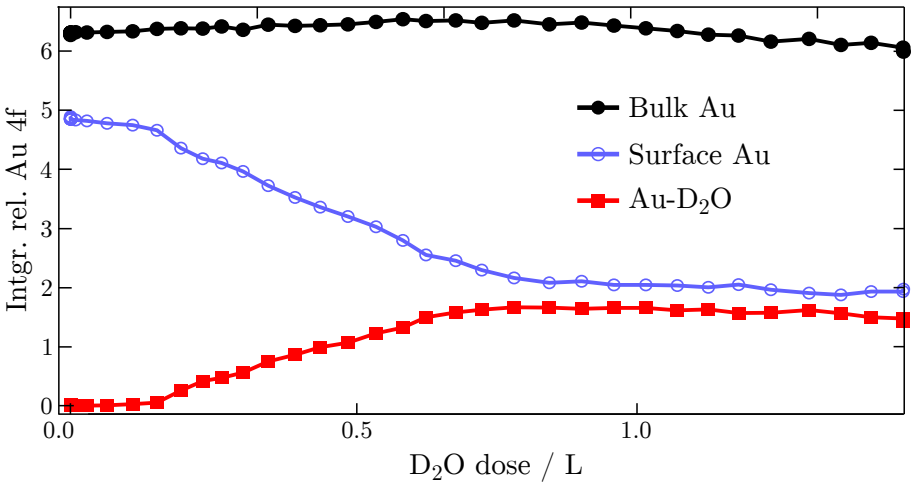

Figure 5.12: Fitted Au $4f_{7/2}$ peak areas plotted versus D_2O dose for the three peaks, assigned to bulk Au (black, solid circles, 84.0 eV), surface Au (blue, open circles, 83.6 eV), and D_2O-bonded Au (red, solid squares, 83.7 eV). Total dose was 1.5 L.

of intact water. For the stepped Au(997) surface, a peak difference of even 37 K was found [223]. No such peak was observed in our experiments.

Van Reijzen et al. [161] show that an electron-irradiated H_2O overlayer forms a high-temperature shoulder in the H_2O desorption spectra. This shoulder was accompanied by the oxidation of CO. The present TPD study did not show such a shoulder to any observable degree.

The XPS data showed (Figure 5.5) that there was a minute peak at 529.9 eV, which we associated with atomic O. However, this peak was around 1 % of the total O 1s signal and could stem from beam damage or dissociation at defects site with even lower coordinated Au atoms. In short, the pristine Au(310) does not significantly dissociate H_2O.

5.4.2 Adsorption and desorption

The second point we address is the validity of desorption experiments to yield information on the adsorption structure of H_2O. Adsorption experiments have a surface temperature of typically tens of kelvin lower than the onset of desorption. This lower temperature opens the possibility that adsorbates stay trapped in a metastable phase. This phase can transform into a more stable phase upon heating the surface. This newly formed phase is probed with TPD and not the original metastable adsorption phase.

This mechanism is believed to explain the discrepancy on Au(111), between desorption and adsorption measurements. On one hand, TPD experiments showed fractional desorption, indicating desorption from ice crystallites and nonwetting behavior [154, 155]. On the other hand, several adsorption experiments resulted in an extended wetting layer [156, 159, 163]. During the temperature increase, a wetting

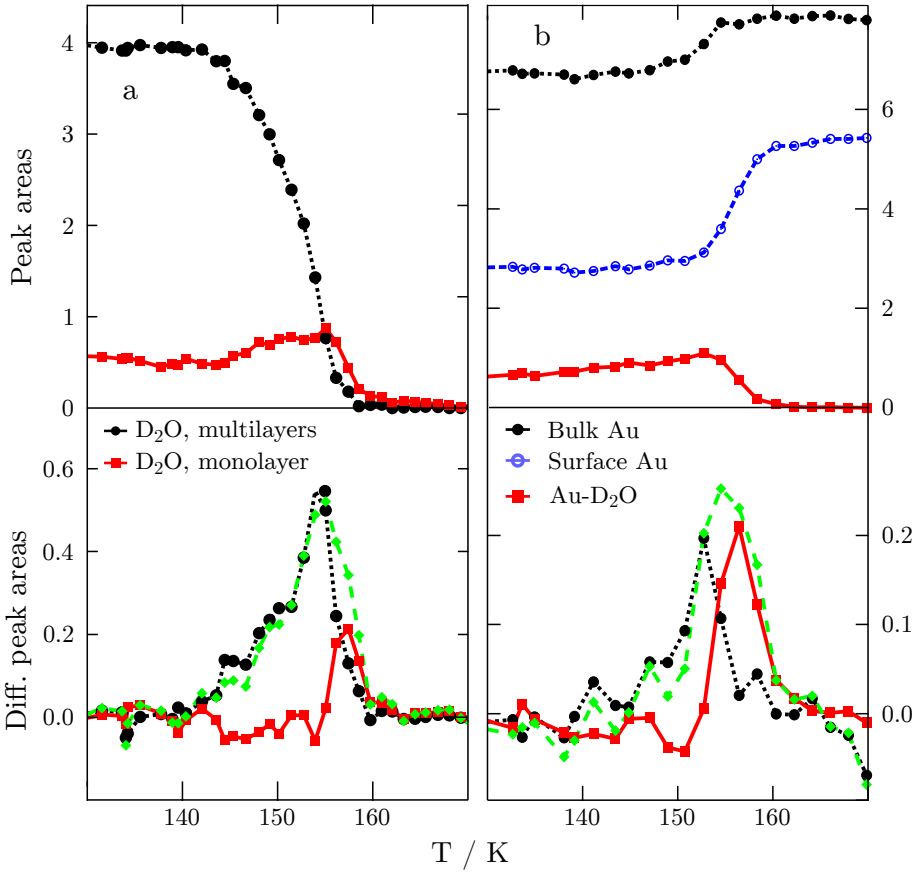

Figure 5.13: Top panels show fitted O 1s (a) and Au $4f_{7/2}$ (b) peak areas during a linear temperature ramp of 0.10 K/s. They show the desorption of D_2O from Au(310). Lower panels display the derivative with respect to temperature mimicking TPD spectra. All derivatives were plotted to yield positive rates. Green traces (dashed) show the total desorption rate.

to non-wetting phase transition occurs, similar to H_2O/Cu(111) [224, 225].

The XP spectra recorded during the temperature ramp (Figure 5.13) indicated no sign of any such transition up to the onset of desorption. However, there was a slight increase in the O 1s 'monolayer' signal and the Au $4f_{7/2}$ D_2O-Au signal. This increase of O 1s 'monolayer' was correlated with decreased shielding of desorbing multilayers.

In conclusion, we observe no changes in adsorption between ∼100 K and the onset of desorption. Therefore, the TPD experiments can be trusted to yield reliable information on the adsorption of H_2O on Au(310).

5.4.3 Monolayer adsorption

Next, we will discuss two interesting features of the TPD traces for (sub)monolayer desorption. The first one is the manifestation in a single peak (in addition to the peak ascribed to bulk desorption). In other words, we will explain the absence of separate terrace and step contributions in the TPD spectra. Second, we will explain the zero-order nature of this peak.

Single desorption peak

When we compare the TPD spectra of Au(111) [154, 155] with the ones obtained from Au(310), the differences are obvious. On Au(111), desorption lacked a distinct (sub)monolayer peak and the desorption order was ∼0.6. Both features demonstrated that 3D ice crystallites were thermodynamically more stable than an extended overlayer. In contrary, there was distinct (sub)monolayer desorption on Au(310) and it desorbed at higher temperatures than ice multilayers. This indicated that an extended (sub)monolayer was more stable than ice crystallites.

The difference in desorption from Au(310) and Au(111) can be related to the presence of steps. These steps directly increase the bonding strength of H_2O on Au as discussed before. In addition, the steps may play a more subtle role in protecting the surface from reconstructing, thus keeping the coordination of the surface atoms lower. Interestingly, the precise step orientation is very important in stabilizing H_2O on Au. Desorption from the stepped Au(997) surface did not result in a separate contribution from (sub)monolayer desorption [223]. Desorption from this surface is remarkably similar to desorption from Au(111). However, both the Au(310) and Au(997) surfaces have steps forming a small (110) facet. The difference between the two steps is the direction of the step with respect to the (110) plane: the steps of the (310) surface run along the $[00\bar{1}]$ direction but the steps of the (997) surface are in the $[\bar{1}10]$ direction.

Surprisingly, no separate contribution from steps and terraces was observed in the TPD experiments, in contrast to desorption from stepped Pt surfaces [185, 186]. This single (sub)monolayer desorption peak on Au(310) was attributed to desorption from (but not limited to) steps, since steps generally bind H_2O stronger than terraces.

This interpretation is supported by a coadsorption study of H_2O and CO [161]. In this work, van Reijzen et al., preadsorbed CO on Au(310), which is believed to occupy steps [161, 208]. Additional H_2O adsorption competes with CO for step sites. This compresses the CO molecules and forces them to occupy closer-spaced step sites.

The absence of a peak originating from terrace-bonded H_2O can be explained by either hydrophobic terraces, which are nonwetting. This would result in nucleation of ice crystallites between steps from which desorption would be similar to desorption on Au(111). A second possibility, however, is desorption from an H_2O structure covering both step and terrace. To explain the single desorption feature in this case, desorption needs to have a single rate-limiting step. This step could be the release of H_2O bonded to steps after which nearby terrace-bonded H_2O instantaneously desorbs.

Zero-order kinetics

The zero-order kinetics of the (sub)monolayer peak is also rather remarkable. This can occur in two separate cases. The first one is adsorbate geometry dependent and occurs when desorption takes place from the end points of 1D structures or from the surface of flat multilayers. The other situation of zero-order desorption results from an equilibrium between condensed island and isolated monomers. If desorption is restricted to the isolated monomers and as long as this equilibrium is maintained, the loss of monomers by desorption is replenished by detachment from the islands. If the size of the islands does not change too much, the concentration of monomers remains (nearly) constant [226]. In both cases, the number of desorption sites is constant, which results in a desorption rate effectively independent of coverage.

Zero-order desorption of H_2O is frequently observed for multilayers and monolayers on *flat* surfaces [174], but on stepped surfaces, examples show that desorption from terraces changes to first order [185, 186]. This occurs when the step density is high enough and terraces too narrow to allow for phase coexistence [227]. In addition, desorption from steps was reported to follow first-order kinetics [184–186].

In our case, the surface had very small terraces and a very high step density but still exhibited zero-order desorption. Instead of a two-phase coexistence model, we propose that desorption occurred from the ends of 1D structures covering either only a step or both a step and (part of a) terrace. This model would also yield zero-order desorption.

The difference between H_2O desorption from stepped Pt and Au surfaces can be explained as follows. For the Pt steps, H bonding between adsorbed H_2O molecules is weaker compared to flat Pt [191, 200] and the Pt-H_2O is relatively strong. This means that desorption could occur from every step site, resulting in first-order desorption. The Au-H_2O interaction, however, is much weaker [228–230] and lateral interactions play a more important role and hinder first-order desorption.

The distance between step atoms in Au(310) is larger than on the stepped Pt(111) surfaces (408 pm for Au(310) and 278 pm for steps on Pt(111)). To have strong lateral interaction and explain the zero-order desorption, it will be necessary that more H_2O is incorporated in the 1D structures on Au(310). The binding of these H_2O molecules could predominantly be with step-bonded H_2O and less with the Au surface. This connective H_2O will most likely directly desorb together with desorption from the step sites. This is consistent with the appearance of a single desorption feature.

XPS data

The O 1s (Figure 5.7) and Au $4f_{7/2}$ (Figure 5.11) XP spectra taken during the uptake of D_2O shed more light on the relative step/terrace coverage of the (sub)monolayer structure.

Remarkably, the D_2O 'multilayer' peak was populated from the start of adsorption (Figure 5.8), which seems completely counterintuitive. Even when molecules were kinetically trapped on top of the first layer, this growth rate at low D_2O dose would not be expected.

Therefore, we propose to ascribe the O 1s 'multilayer' peak to weakly bonded

D_2O. This D_2O could reside both in multilayers and in the (sub)monolayer. For D_2O in the (sub)monolayer, this could be D_2O bonded to the ninefold coordinated Au atoms. Similarly coordinated atoms are also present on Au(111) and are the most predominant atoms on Au(997). On these surfaces, H_2O adsorption shows single, symmetric peaks with a binding energy of 533.2–532.6 [221, 231, 232] and 532.7 eV [223], respectively. These values are very close to the peak at 532.8 eV, which we assign to D_2O bonded to ninefold coordinated Au atoms. A contribution from D_2O bonded to ninefold coordinated Au atoms was absent in the TPD measurements. This could indicate that they desorbed at the same temperature as multilayer D_2O or that they diffused to six- and eightfold binding sites during the temperature ramp.

The initial growth rate of weakly bonded D_2O was half that of the 'monolayer' O 1s peak (Figure 5.8). The latter could be ascribed to D_2O bonded to both the six- and eightfold coordinated Au atoms and reached a maximum of 0.6 ML. This was a bit lower than the expected value of 0.67 ML, which could be explained by shielding by the second layer of D_2O.

The second-layer D_2O was indistinguishable with XPS from that of the weakly bonded D_2O in the (sub)monolayer. It started growing at a coverage of 0.9 ML after dosing 0.4 L. At this point, around 80 % of the ninefold coordinated Au atoms were populated.

Inspired by previous research [168, 181], we overlaid several possible adsorption geometries with the (310) surface (Figure S2). These models agree with our findings; however, without structural information we will not speculate further.

To sum up, both Au $4f_{7/2}$ and O 1s XP spectra suggest that the (sub)monolayer adsorption consisted of differently bonded species, but the ratio between the species remained difficult to determine exactly.

5.4.4 Multilayer adsorption

Finally, we discuss the adsorption and desorption of multilayer H_2O from this surface. This desorption occurred at typical temperatures for multilayer desorption. Furthermore, the observed zero-order behavior was not unexpected (Figure 5.3b). However, the calculated binding energy (48 ± 1 kJ/mol) (Figure 5.4) was somewhat higher than that for desorption of ice clusters from Au(111) (44 kJ/mol) [154].

Starting from the second layer, the adsorbed H_2O could form 3D clusters on the surface. In this case, a two-phase coexistence with monomers adsorbed on the first layer would explain the zero-order behavior.

An alternative view can be derived from the adsorption of H_2O on Au(115) [160, 162]. On this surface, vibrational features remained nearly constant up to at least the tenth layer. These vibrational signatures suggested that the monolayer structure extended in the following layers.

A similar argument could apply on Au(310). If the high step density increased the formation energy of ice clusters, it could be energetically favorable for the multilayers to adapt to the monolayer structures. The multilayer structures could be stabilized by H bonding to the monolayer structures. These H bonds could originate from the upwardly sticking O-H bonds in the first layer.

5.5 Summary and conclusions

The interaction between H_2O and the stepped Au(310) surface differed significantly from the hydrophobic Au(111) surface. Our findings obtained with TPD and XPS are summarized as follows:

1. Steps did not dissociate H_2O. They did make the surface hydrophilic.
2. The precise orientation is very important in stabilizing H_2O: (110) steps parallel to $[00\bar{1}]$ as found on Au(310) bind H_2O significantly more strongly than (110) steps in the $[\bar{1}10]$ direction.
3. The observed desorption behavior can be explained by 1D adsorption structures.

The presence of steps led to a distinct (sub)monolayer desorption peak. The observed zero-order kinetics was rationalized by desorption occurring only at the ends of 1D structures.

During desorption, no separate contribution from steps and terraces was detected. In addition, XPS results suggested that H_2O occupies multiple adsorption sites. To explain these observation, we propose that 1D structures covered the steps and also (part of) the terrace. These structures were stabilized by step-bonded H_2O. Desorption of the step-bonded H_2O was rate limiting and resulted in a single desorption peak.

In addition, XPS measurements showed no dewetting transition while heating the surface, as was found on Au(111) and Cu(111). Furthermore, XP spectra showed no significant interaction between additional H_2O layers and the Au surface. These additional layers could either have formed clusters or 1D structures, dictated by the monolayer structures.

Supplementary information – Hydrophilic interaction between low-coordinated Au and water

TPD Simulation

A temperature-programmed desorption (TPD) simulation was performed to gain further insight into the observed desorption kinetics. For this simulation, the coverage and desorption rate were evaluated for the experimental temperature range with different initial coverages by calculating

$$R_{des} = \theta^n A \exp(-E_a/RT)$$

In this formula, θ is the actual coverage, numerically calculated from the initial coverage, n is the desorption order, and A is the pre-exponential factor (estimated to be 1×10^{13}). The H_2O adsorption energy of peak β and a heating rate of 0.9 K/s were used. This simulation was repeated for desorption orders of 0, 1/2, 2/3, and 1.

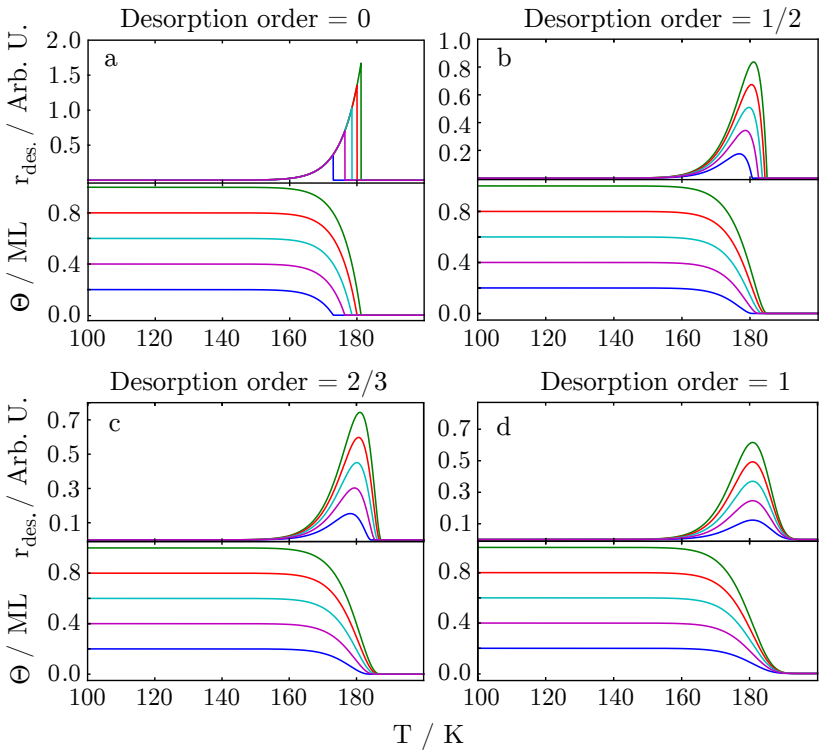

Figure 5.14: Four simulated TPD experiments showing the effect of the desorption order on the coverage dependence of the desorption rate. These desorption rates are depicted in the top panels and plotted versus temperature, while the lower panels show the temperature-dependent coverage. For every simulations, five initial coverages between 0 and 1.0 ML were used. From left to right, the panels show the desorption behavior for desorption orders of 0, 1/2, 2/3, and 1. Indicative of zero-order desorption are the completely overlapping leading edges and desorption peaks on the leading edges.

First-order desorption occurs when intact molecules desorb without any complicating intermolecular interaction. Fractional desorption is expected when desorption results from the perimeter of either islands (n = 1/2) or clusters (n = 2/3). Zero-order desorption can occur in two separate cases. The first one is adsorbate-geometry dependent and follows when desorption takes place from the end points of 1D structures or from the surface of flat multilayers. The other situation of zero-order desorption results from an equilibrium between condensed island and isolated monomers. If desorption is restricted to the isolated monomers and as long as this equilibrium is maintained, the loss of monomers by desorption is replenished by detachment from the islands. If the size of the islands does not change too much, the concentration of monomers remains (nearly) constant [226]. In both cases, the number of desorption sites is constant, which results in a desorption rate effectively independent of coverage.

When the four simulation are compared, the differences between zero and first-order desorption kinetics are striking. First-order desorption shows non-overlapping leading edges and maximum desorption temperatures independent of coverage. On the other hand, zero-order desorption shows overlapping leading edges and desorption temperature shifting to higher temperatures. Fractional desorption gives intermediate behavior between these extreme cases.

A comparison of the simulated (Figure 5.14) and the experimental (main text, Figures 5.2 and 5.3) TPD traces reveals that the experimental peaks show complete zero-order desorption kinetics.

Proposed Models

All experimental results can be explained by (sub)monolayer adsorption in 1D structures or chains with strong H bonding along the chain. However, the nearest-neighbor distance between step atoms in Au(310) is large and disfavors strong H bonds. Therefore, it is unlikely that H_2O adsorbs in chains that only cover the step atoms as on Pt [199, 204, 205].

Figure 5.15 shows three models inspired by previous research [168, 181] overlaid on the Au(310) surface. First, a model covering the step sites and an equal number of terrace atoms to facilitate H bonding is shown in Figure 5.15a. Lin and Gross showed that this is the most stable structure formed on unreconstructed Au(100) [168].

The second and third model depicted in Figures 5.15b and c are adapted from the structures proposed by Carrasco et al. for H_2O on Ag(110) and Cu(110), respectively [181]. According to Carrasco et al., the lattice constant of the metal substrate determines the preference to either form chains built from hexagons (Ag) or pentagons (Cu). Following this reasoning, the (unreconstructed) Au(110) would adopt a hexagon-based structure. However, there is significant difference between the (110) and the stepped (310) surface. This leads to hexagons spanning three planes and the pentagons spanning two. This buckling can have detrimental consequences on the relative stability between the hexagons and pentagons and on their total stability. Another complication arises when all steps are covered. In this case, H_2O molecules at the outer corners of the hexagons are shared between chains. This is not the case for the pentagon

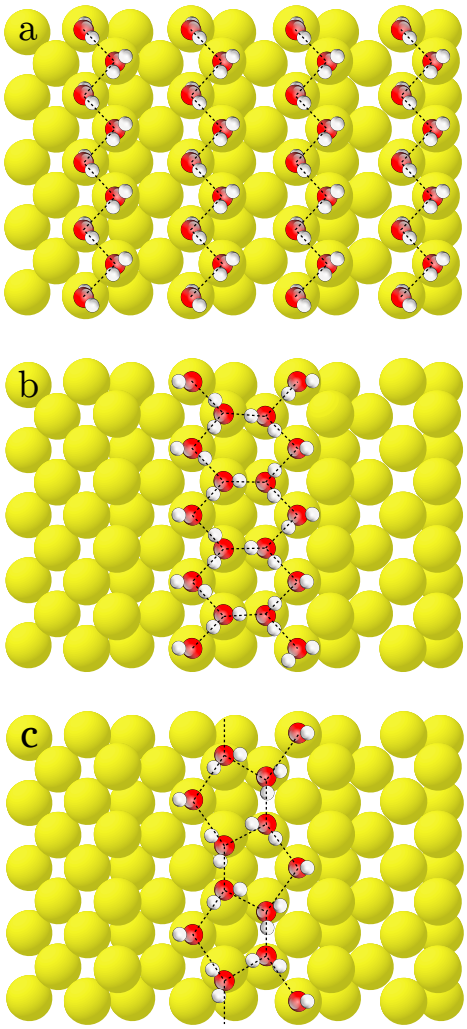

Figure 5.15: Three possible H_2O adsorption geometries overlaid on a (310) surface [206]. No structural optimization was performed. (a), based on DFT calculation on unreconstructed Au(100) [168]. (b), based on DFT calculations on Ag(110) [181]. (c), based on STM and DFT calculations on Cu(110) [181].

chain, but also here lateral interactions between chains can play an important role.

Without further research, we will not try to predict relative stabilities of the three models. Structural measurements, such as scanning tunneling microscopy (STM), in combination with density functional theory (DFT) calculations, are needed to give further insight into the (sub)monolayer adsorption of H_2O on Au(310).